Hindawi
Advances in Materials Science and Engineering
Volume 2023, Article ID 9820671, 1 page
https://doi.org/10.1155/2023/9820671

Retraction

Retracted: Process Optimization of Spark Plasma Sintering Parameters for Tungsten Carbide/Silicon Nitride/AA2219 Composites by Taguchi Method

Advances in Materials Science and Engineering

Received 26 December 2023; Accepted 26 December 2023; Published 29 December 2023

This article has been retracted by Hindawi, as publisher, following an investigation undertaken by the publisher [1]. This investigation has uncovered evidence of systematic manipulation of the publication and peer-review process. We cannot, therefore, vouch for the reliability or integrity of this article.

Please note that this notice is intended solely to alert readers that the peer-review process of this article has been compromised.

Wiley and Hindawi regret that the usual quality checks did not identify these issues before publication and have since put additional measures in place to safeguard research integrity.

We wish to credit our Research Integrity and Research Publishing teams and anonymous and named external researchers and research integrity experts for contributing to this investigation.

The corresponding author, as the representative of all authors, has been given the opportunity to register their agreement or disagreement to this retraction. We have kept a record of any response received.

References

[1] S. Althahban, G. Pathinettampadian, F. Qahtani et al., "Process Optimization of Spark Plasma Sintering Parameters for Tungsten Carbide/Silicon Nitride/AA2219 Composites by Taguchi Method," *Advances in Materials Science and Engineering*, vol. 2022, Article ID 4829499, 8 pages, 2022.

Hindawi
Advances in Materials Science and Engineering
Volume 2022, Article ID 4829499, 8 pages
https://doi.org/10.1155/2022/4829499

Research Article

Process Optimization of Spark Plasma Sintering Parameters for Tungsten Carbide/Silicon Nitride/AA2219 Composites by Taguchi Method

Sultan Althahban,[1] Gurusamy Pathinettampadian,[2] Faez Qahtani,[3] Yosef Jazaa,[4] S. Mousa,[5] Sanipina Anjani Devi,[6] Melvin Victor De Poures,[7] R. Subbiah,[8] and Hana Beyene Mamo [9]

[1]*Department of Mechanical Engineering, Jazan University, Jazan 82822, Saudi Arabia*
[2]*Department of Mechanical Engineering, Chennai Institute of Technology, Chennai, Tamilnadu, India*
[3]*Department of Mechanical Engineering, Najran University, Najran-11001, Saudi Arabia*
[4]*Faculty of Engineering, King Khalid University, Abha 62529, Saudi Arabia*
[5]*Faculty of Engineering, Jazan University, Jazan 706, Saudi Arabia*
[6]*Department of Mechanical Engineering, Aditya Engineering College, Surampalem 533437, Andhra Pradesh, India*
[7]*Department of Thermal Engineering, Saveetha School of Engineering, Saveetha Institute of Medical and Technical Sciences, Chennai, Tamilnadu, India*
[8]*Department of Mechanical Engineering, Gokaraju Rangaraju Institute of Engineering and Technology, Telangana, India*
[9]*Faculty of Mechanical Engineering, Jimma Institute of Technology, Jimma University, Jimma, Ethiopia*

Correspondence should be addressed to Hana Beyene Mamo; hana.beyene@ju.edu.et

Received 6 June 2022; Revised 22 July 2022; Accepted 4 August 2022; Published 30 September 2022

Academic Editor: K. Raja

It is usual practice to optimize the various processing parameters in order to achieve well-organized and lucrative process conditions. For the creation of tungsten carbide/silicon nitride/AA2219 composites, sintering temperature, sintering pressure, dwelling time, and heating rate all must be optimized. Design of experiments and analysis of variance were employed to assess the factors' contributions to density as well as microhardness response variables. It was decided to test the admixed powders and Vickers hardness tester, optical microscope, and Archimedes-based density testing to evaluate the sintered compacts. The optimum spark plasma sintering factors were a temperature of 500°C, a pressure of 30 MPa, a dwelling time of 8 minutes, and a heat rate of 160 °C/min, resulting in an extreme density of 2.71 g/cm^3 and a maximum microhardness of 38.61 HV (0.38 GPa).

1. Introduction

Low power consumption and quick processing times have made nonconventional spark plasma sintering (SPS) an increasingly popular sintering method [1]. MMCs and MMNCs can be fully densely consolidated at low temperatures, despite the fact that this process is still relatively new [2]. Although spark plasma sintering was first described by [3], it is now widely accepted that the rapid sintering technique was invented by them. Spark plasma sintering utilizes heat to rapidly sinter a powder compact on a macroscopic level, but it is also used at microscopic levels to deliver energy to the powder particles' contact points [4]. When combined with plasma generation, resistive heating, and pressure application, spark plasma sintering has been proven to accomplish very rapid sintering [5]. Since the microstructure is regulated and grain development is minimal or nonexistent during the brief sintering period [6], the composite has better mechanical and thermal properties as well as chemical qualities. While other processes like SPS eliminate porosity and coarsen the microstructure of the material, spark plasma sintering minimizes the number of

contaminants like H_2 and O_2 [7]. Numerous commercial uses have been described in the scientific literature for the usage of aluminum reinforced with a hard-secondary phase [8, 9]. In engine cylinders, rotors, commercial products, and wear application systems for all these composite materials have been shown to be effective [10].

SPS of aluminium reinforced with carbon nanotubes [11] has received a large amount of attention, but the ternary tungsten carbide/silicon nitride/AA2219 nanocomposites have received little or no attention at all. When employing 500°C, 30 minutes, 30 MPa, 5 Pa vacuum and cooling rate of 500°C per minute, an SPS of [12] AA2219-tungsten carbide AA2219-tungsten carbide resulted in 300 MPa, more than three times the strength of AA2219. As a result, a number of studies are presently focused on discovering the optimum way to disperse the great features of WC on the Al matrix for use in microelectronic and electrical, energy, health, and structural applications [13]. Many writers have indicated that silicon nitride is an excellent alloying material for aluminum. A thin interdendritic flick of yielding aluminium, which sustains strains, and the occurrence of silicon nitride, which hinders crash circulation, were cited by [14, 15] as the reason for no cracking on the surface of their spark plasma sintered Al-Nb composite. Additionally, silicon nitride has been shown to exhibit exceptional fracture toughness, superb superconductivity, and great thermal and corrosion resistance in other studies [16, 17]. As a result, the properties of tungsten carbide and silicon nitride are expected to provide aluminium with higher strength, electrical and thermal conduction, and superior corrosion and wear resistance, for a wide range of engineering uses [18].

MMCs have been overtaken by nanocomposites due to their superior properties, including greater toughness, lesser granular size, best wear and abrasive properties, enhanced toughness, ductileness, and exhaustion resistance [19]. In order to attain full density while conserving resources, adjusting these factors is essential. To ensure that the theoretical density of the composite is reached at minimal input factors, process parameters play an important role in experimental research [20, 21]. Al-1wt% SiC microhardness of 108 MPa and compressive strength of 312 MPa were achieved with the ideal factors of 450°C temperature, 8 minutes of dwelling time at 45 MPa pressure, and 160°C/min heat rate, according to [22, 23]. It is possible to reduce expenses and time and energy by reducing the amount of trial-and-error in experiments. Tungsten carbide/silicon nitride/AA2219 composite process parameters have received far less attention than optimization of SPS parameters [24]. Researchers in this study are utilizing ANOVA and design of experiments to refine the spark plasma sintering parameters of this composite [25]. Thus, this research makes use of spark plasma sintering process with different input parameter through Taguchi, and the corresponding mechanical properties like density and microhardness are studied for useful application.

2. Materials and Methods

2.1. Materials. The 99.5%marketable aluminum 2219 was used as the study's starting metal. The most frequent material is used to construct liquid cryogenic rocket fuel tanks. It features one-of-a-kind mix of qualities, including outstanding cryogenic capabilities. Tungsten carbide was utilized as a reinforecement with the size of 10-30 nm. Alloy 2wt%, 2wt% WC, and 2wt% silicon nitride were combined in a dry atmosphere utilizing the Turbular Shaker Mixer model T2F for 10 hours at 110 rpm in order to ensure that the powders were thoroughly mixed. While mixing, it was required to add approximately steel balls (4 mm radius) to the vessel of powder so that the reinforcement could be better dispersed in its matrix [2].

2.2. Design of the Experiment. Taguchi devised a typical type of DOE known as the Taguchi technique, which is more accessible and economically viable because of the huge reduction in experimental time and expense [26, 27]. By maintaining consistency of performance and reducing variation, it is an excellent tool for optimizing process design. For the best possible responses to process variables, this powerful tool utilizes three design processes: system design, parameter design, and tolerance development [28, 29]. As a first step in the development process, system designers must identify the most critical design variables and then determine the range of acceptable values for each one. Parameter design, also known as robust design, discovers the best values for design parameters in order to reduce the effects of variance and noise [30]. Tolerance design is used to tighten tolerances in parameter design in order to acquire the best results. By employing Taguchi's orthogonal array (OA) architecture, the manageable constraints can be evaluated with their associated answers at multiple stages in an ordered way [31]. This reduces both time and money.

2.3. Taguchi Method. Taguchi technique was used in this work because it is an effective tool for constructing trials when numerous variables are to be optimized, as is the situation with spark plasma sintering [32]. Because the number of tests is minimized, this method is often preferred to the factorial design method because it saves both time and money. It is thus possible to limit the number of tests by eliminating combinations of variables that are unnecessary, leaving just the most crucial combinations of parameters at their proper levels in the Taguchi's orthogonal array experimentation method [31]. There are four factors to consider in this experiment: sintering temperature, pressure, and dwell time, as well as heating rate, all of which are shown in the table at three different levels. Respondent variables include sintered composite densities and microhardness. It was also found that the process variables were statistically significant thanks to an analysis of variance (ANOVA). Table 1 is constructed using the Taguchi L_9 orthogonal array, yielding a total of nine experiments [33]. The following is the outcome: Minitab 16.1 was used to create the experiment, and the Taguchi option was used, as previously stated. Factor variables are the scientific term for the study's four main sintering parameters. Temperature, pressure, dwell time, and heating rate were all taken into consideration. Each of the following variables was considered at three different levels:

Table 1: Taguchi's L_9 arrangement.

Experimental trials	**Sintering temperature** (A)	**Pressure** (B)	**Dwellingtime** (C)	**Heatingrate** (D)
1	1	1	1	1
2	1	2	2	2
3	1	3	3	3
4	2	1	2	3
5	2	2	3	1
6	2	3	1	2
7	3	1	3	2
8	3	2	1	3
9	3	3	2	1

temperature (400°C), pressure (30 Mpa), dwell duration (12 minutes), and heating rate (240°C). The "factor variable" number was typed into a pop-up box, then the "level" number was entered into a pop-up box, and then ok was clicked to enable the program to begin. There are four columns in the table: temperature (A), pressure (B), dwell time (C), and heating rate(D). It was clear that steps 1 through 3 were recurrences across the data. It is possible to perform nine tests by entering varying values for three parameters: 1, 2, and 3. This yields the lowest, medium, and highest possible results.

2.4. Sintering Process Using a Spark Plasma. The KCE-FCT-HHPD 25 spark plasma sintering equipment was used in this work with a vacuum pressure of 0.605 bar, a relative pressure of 500 bar, and an absolute pressure of 1.2 bar. Before beginning sintering, the machine was calibrated to these settings. As needed, the admixed powder was weighed out to generate nanocomposites with a 15 mm radius and 5 mm thickness. Sintering with the settings is shown in Table 2. For simpler exclusion of sintered specimen and to eliminate temperature + gradients, graphite sheets were used to hide powders from the die and the upper and lower punches [34]. A total of nine samples were gathered and analyzed, as shown in the design table.

2.5. Testing on Density. For estimating the density of the specimen, we used the Archimedes method, whereas equation (1) was used to get the starting powder's bulk density. Using a rule of mixes formula, the relative density of the powdered constituents was calculated using the theoretical bulk density.

$$\rho bulk = \left\{ \frac{\%Al}{\rho_{Al}} + \frac{\%WC}{\rho_{WC}} + \frac{\%Si_3N_4}{\rho_{WCSi_3N_4}} \right\}^{-1}, \quad (1)$$

where $\rho_{\text{bulk}}, \rho_{Al}, \rho_{WC,}$ and ρ_{Si3N4} are densities of bulk, aluminium, tungsten carbide, and silicon nitri de, respectively.

2.6. Testing on Microhardness. Samples of the AA2219-2% WC-2% Si_3N_4 composites were examined on a Vicker's microhardness tester (FM-800) using a diamond indenter with a force of 100 g for 16 seconds and a 0.1 spacing.

Table 2: Design of the experiment.

Experimental trials	Temperature (°C)	Pressure (**MPa**)	Dwelling time (**min**)	Heat rate (°C/ min)
A	400	15	8	80
B	400	30	12	160
C	400	45	16	240
D	450	15	12	240
E	450	30	16	80
F	450	45	8	160
G	500	15	16	160
H	500	30	8	240
I	500	45	12	80

3. Results and Discussion

In spark plasma sintering, little grain growth occurs even when the material is fully densified. Densification in these samples is attributed entirely to the complete removal of pores and grain boundaries. As seen in [35], this consolidation process is powerful enough to assure strong adhesion among the matrix and reinforcements, resulting in the high hardness and full densification of this composite. Using this technique in conjunction with the best process conditions, a composite with zero porosity and impurities can be created.Saying that spark plasma sintering is unique among fabrication methods is pointless. This is due to the tensile strength of 115 MPa obtained [36] during the induction melting of AA2219-WC.

AA2219-tungsten carbide plasma spurting by [37] had a tensile strength of 83.2 MPa, which was the highest. A hardness of 38.61 HV (381.2 MPa) was achieved, which is corresponding to tensile strength of 125.4 Mpa. Sintered samples' densities are shown in Table 3, though the ANOVA outcomes are shown in Table 4. Sintering sample density is illustrated in Figure 1 as an interplay between predictor factors. Figure 1(a) depicts the most significant graphic for relative density. The relative density amplified from 87% to 99% when the sintering temperature increased from 400 °C to 450 °C. After a further rise in temperature, the average density had reached a whopping 99.5%. In addition, a rise in pressure from 15 to 30 mega Pascal raised the comparative density from 96 to nearly 99% on the pressure plot. However, when the pressure was bigger to 45 MPa, the line began to decline by roughly 96%.

Table 3: Density and microhardness testing results.

Trial no.	Density (g/cm^3)	Relative density (%)	Microhardness (HV)
1	2.39	89.3	26.92
2	2.61	96.3	36.42
3	2.43	89.7	28.45
4	*2.72*	*97.5*	37.63
5	2.65	98.8	32.18
6	2.69	99.4	36.56
7	2.68	97.8	38.61
8	2.68	98.8	38.53
9	2.71	99.5	39.04

Table 4: ANOVA results on density.

Factors and interaction	F value	P value	Involvement	R squared (%)
Sintering temperature (*A*)	11.66	0.008	28.2	79.81
Pressure (*B*)	0.21	0.832	–	
Dwelling time (*C*)	0.14	0.883	–	
Heating rate (*D*)	0.35	0.731	–	86.03
AB	10.15	0.012	23.6	84.47
AC	4.87	0.017	12	89.07
AD	28.98	0.005	42	
BC	0.014	0.797	–	
BD	0.037	0.699	–	
CD	0.024	0.732	–	

There is a significant increase in relative density between 8 and 12 minutes and a fall between 16 and 24 minutes on the time plot. At 240°C/min, relative density peaked at 80 °C/min, and then fell back to zero, once the heat rate was improved more to 240 °C/min. This plot shows that the ideal density was achieved at 500°C, 30 MPa, 8 min of dwell time, and a heating rate of 160 °C/min. The primary effect plot of means for the signal to noise ratio in relation to density can be seen in Figure 1(b). The study was done using the "bigger is better" option, and the best density was found at 500°C, 30 MPa pressure, 8 minutes dwell time, and a heating rate of 160 °C/min on the main effect plot. With [38] who sintered AA2219-tungsten carbide at 500 °C, 30 minutes, achieved an improved toughness of further than three times that of pure aluminium, which is consistent with our results (85 MPa).

However, complete densification was achieved in 8 minutes rather than 15 minutes in the current investigation. Sintering temperatures over 500°C were not a possibility in this study since an SPS of AA2219-3 wt% tungsten carbide at 500 °C yielded a density of 96%, which suggests that, at 500°C, resident melting of aluminium may have begun, resulting in the drop-in density. Using the table, it can be observed that features A, AB, AC, and AD are important typical relations because they all have *P* values less than 0.05. In order to achieve a fully dense tungsten carbide/silicon nitride/AA2219 composite, these are the most important characteristics to regulate. Temperature contributed 27.5% to the *P* value of 0.009 and had an R-squared value of 79.76% for component A. The sintering temperature, then, is all that matters for predicting the final density, with an accuracy of 79.76% when it comes to predicting the density of a sample. Assuming that temperature variance is significantly different from other parameters, the substitute suggestion that temperature has an important impact on densities can be accepted.

This interaction between temperature and pressure had a R squared value of 86.3%; temperature and time had a R squared value of 0.016%; the temperature and heating rate had a R squared value of 89.7%; and temperature and pressure had a R squared value of 0.011%. One-way ANOVA models and the interactions between two components were the only models examined in this study (two-way). ANOVA results for factors related to microhardness are displayed in Table 5. There is an R-squared value of 63.64% and an R-squared value of 0.048 for the temperature. Microhardness may be predicted with 63.64% accuracy by determining the sintering temperature, which considered for 15.91% of the variables that influence the microhardness. This study found that both the AC and the AD contribute significantly to the total, with AC contributing to 58.61% of the total and AD contributing to 25.63% and R-squared value of 64.81%, respectively.

The rise in the microhardness of the sintered specimen may have been influenced by the variables listed above with *P* values less than 0.05. Temperature rises from 400 °C to 450 °C resulting in upsurge in average microhardness from 29 HV to 38 HV, according to Figure 2 which consists of ANOVA results. Temperature increases from 450 to 500°C caused in 39 HV increases. Proceeding the pressure, a rise in pressure from 15 to 45 MPa resulted in an upsurge of 35 HV

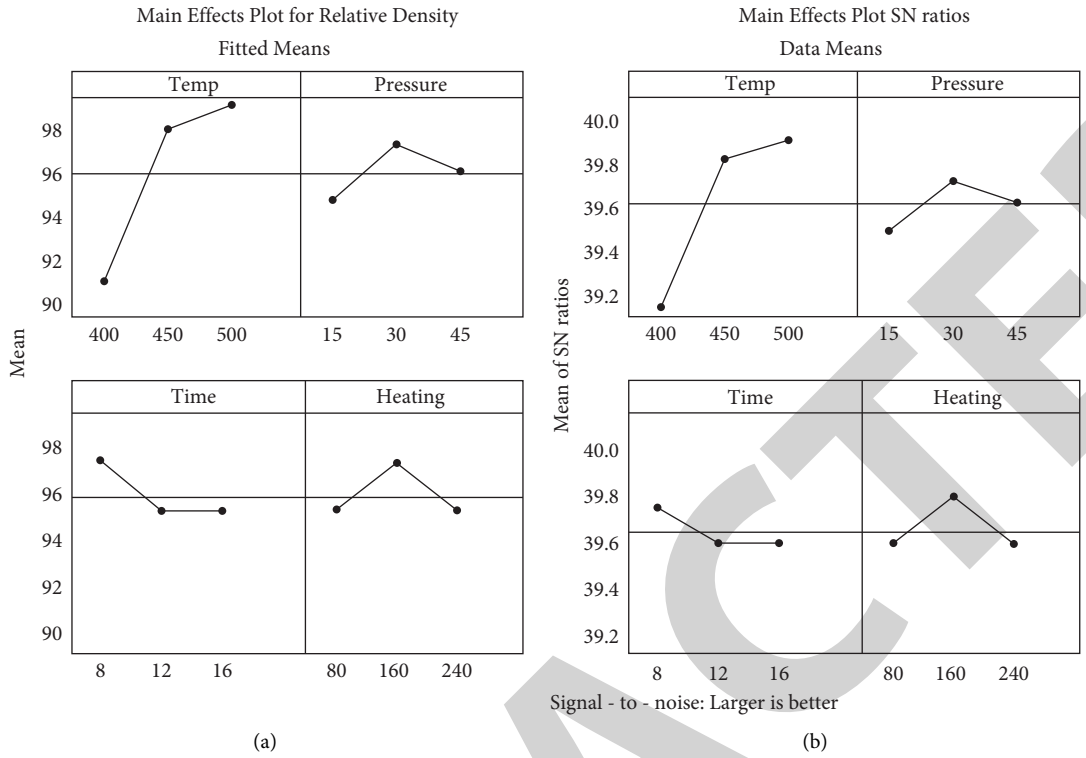

Figure 1: Relative density main effect plot of (a) means and (b) signal to noise ratio.

Table 5: ANOVA results on microhardness.

Factors and interaction	*F* value	*P* value	Contribution (%)	*R*-squared
A: sintering temperature	5.26	0.049	15.91	64.81
B: sintering pressure	0.12	0.908	–	
C: dwelling time	0.66	0.563	–	
D: heating rate	0.55	0.609	–	
AB	0.74	0.098	–	
AC	13.29	0.014	58.61	
CD	0.25	0.414	–	
BC	0.05	0.623	–	
AD	8.78	0.022	25.63	
BD	0.04	0.657	–	

to 37 HV. Microhardness decreased to 33 HV when the pressure was improved to 45 MPa (0.32 GPa). Increase in the temperature from 80 to 160 ˚C/min resulted in a rise from 33 (0.32 GPa) to 36 HV on the heating rate (0.35 GPa). However, increasing the rate of heating to 240 ˚C/min resulted in a downward trend. The time plot indicated a small rise in mean microhardness from 35 HV to 36 HV as the duration increased from 8 to 12 minutes (0.34 GPa). However, increasing the timer to 15 minutes had the opposite effect. The maximum microhardness was achieved at a temperature of 500 ˚C, a pressure of 30 MPa, a dwell duration of 8 minutes, and a heat rate of 160 ˚C/min. According to figures, a higher SN ratio is preferable, and the maximum microhardness was obtained by heating the sample to 500 ˚C for 8 minutes at 30 MPa pressure and heating it at 160 ˚C/min for a dwell duration of 8 minutes.

Sample densities and microhardness process parameters are plotted in Figure 3. High and low density and microhardness were obtained at 500˚C and 400˚C, respectively. There was a clear correlation between microhardness and density at 30 MPa. The two response variables decreased as the pressure was raised more. Figure 3 shows the graph bending inward, indicating that 8 minutes of dwell time yielded the best results. The response variables decreased when the time was increased from 12 to 16 minutes. A heat rate of 160 ˚C/min produced the greatest results.

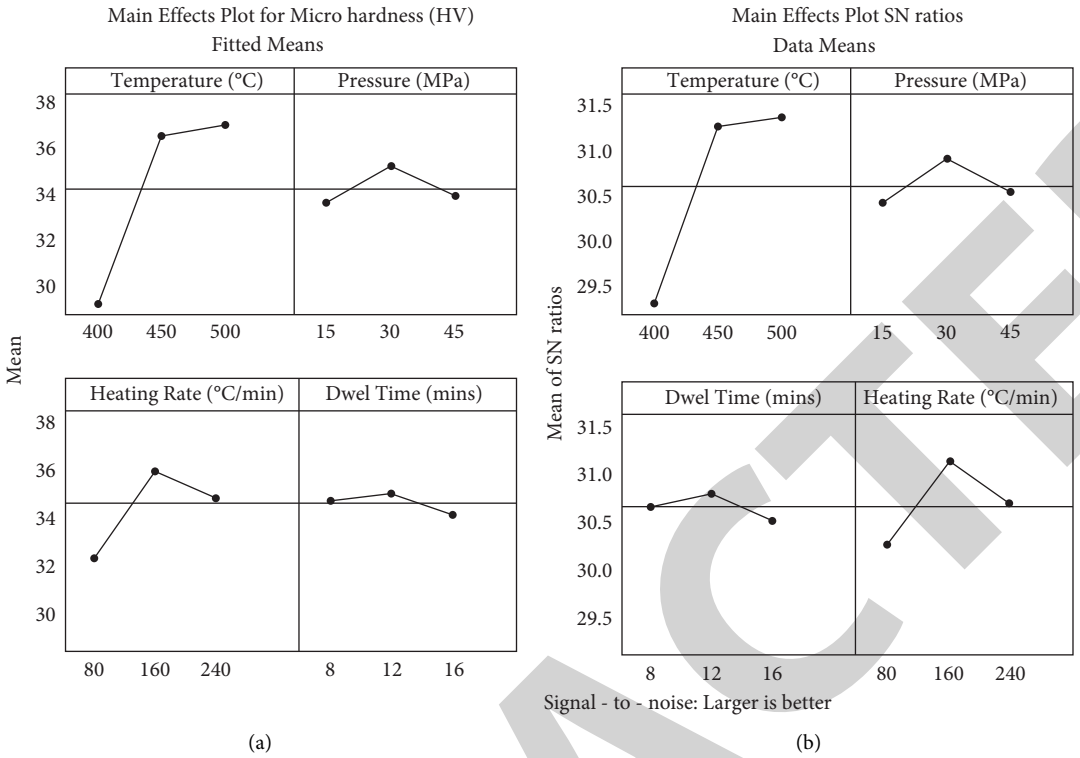

Figure 2: Microhardness main effect plot. (a) Means. (b) Signal to noise ratio.

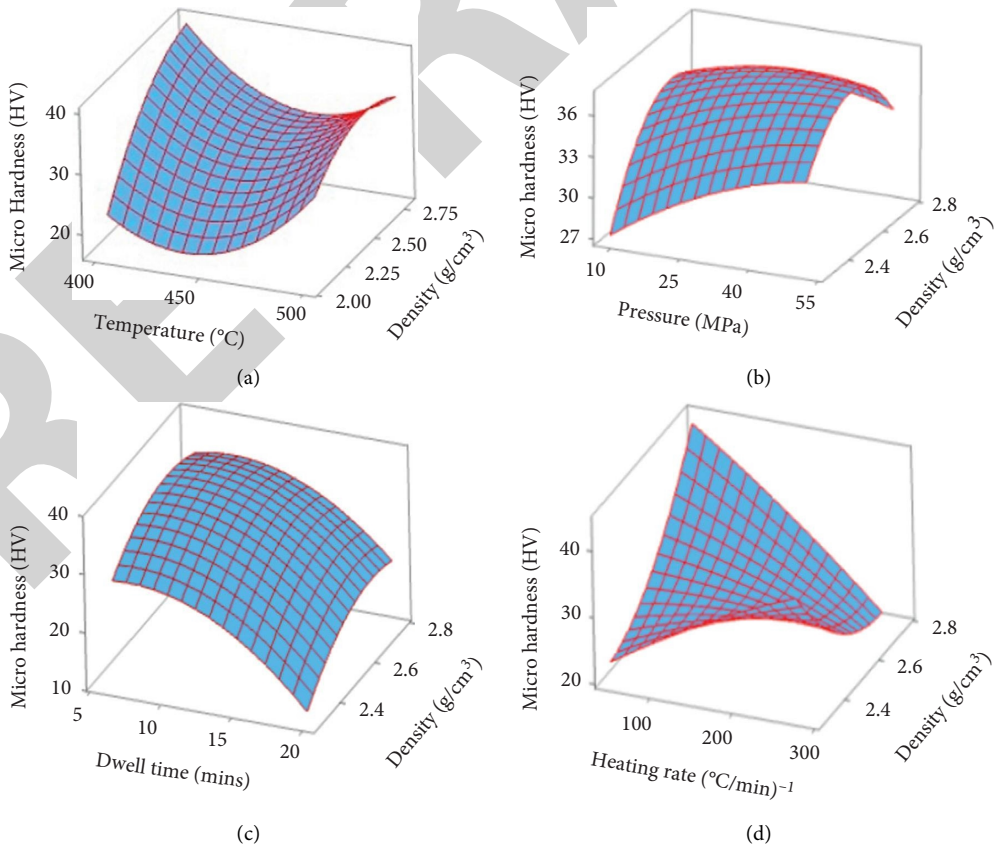

Figure 3: Impact of processing factors on the density and microhardness of AA2219-2%WC-2% silicon nitride: (a) temperature, (b) pressure, (c) dwell time, and (d) heating rate.

4. Conclusion

Spark plasma sintering has been employed to successfully create a nanocomposite of tungsten carbide, silicon nitride, and AA2219, and the following discussion is given as follows:

(1) With the incorporation of 2wt.% silicon nitride into AA2219 powder using spark plasma sintering, the microhardness was enhanced by up to 20% which is useful for a wide range of technical applications, and it was strongly influenced by factors such as temperature, dwell time, and heating rate.

(2) Density and microhardness decreased as pressure, dwelling time, and heating rate are between 30 and 45 MPa, 12 and 16 minutes, and 160 and 240 °C/min, correspondingly. According to the optimization results, the sintering parameters of 500°C temperature, 30 MPa pressure, 12 min dwell time, and 160 °C/min heating rate were found to be best for both density and microhardness.

Data Availability

The data used to support the findings of this study are included within the article. Further dataset or information is available from the corresponding author upon request.

Conflicts of Interest

The authors declare that there are no conflicts of interest regarding the publication of this paper.

Acknowledgments

The authors appreciate the supports from Jimma University, Ethiopia, for the research and preparation of the manuscript. The author thankfully acknowledge the funding provided by Scientific Research Deanship, King Khalid University, Abha, Kingdom of Saudi Arabia, under the grant number R.G.P.1/267/43.

References

[1] A. Das and S. P. Harimkar, "Effect of graphene Nano plate and silicon carbide nanoparticle reinforcement on mechanical and tribological properties of spark plasma sintered magnesium matrix composites," *Journal of Materials Science & Technology*, vol. 30, no. 11, pp. 1059–1070, 2014.

[2] S. Diouf and A. Molinari, "Densification mechanisms in sparkplasma sintering: effect of particle size and pressure," *Powder Technology*, vol. 221, pp. 220–227, 2012.

[3] S. Lin and W. Xiong, "Microstructure and abrasive behaviors of TiC-316L composites prepared by warm compaction and microwave sintering," *Advanced Powder Technology*, vol. 23, no. 3, pp. 419–425, 2012.

[4] M. Suarez, M. A. Fernandez, J. L. Menendez et al., "Challenges and opportunities for spark plasma sintering: a key technology for a new generation of materials B," in *Sintering Applications*, Ertug, Ed., InTech, Rijeka, Croatia, 2013.

[5] N. S. Weston, F. Derguti, A. Tudball, and M. Jackson, "Spark plasma sintering of commercial and development titanium alloy powders," *Journal of Materials Science*, vol. 50, no. 14, pp. 4860–4878, 2015.

[6] H. Feng, Y. Zhou, D. Jia, and Q. Meng, "Rapid synthesis of Ti alloy with B addition by spark plasma sintering," *Materials Science and Engineering A*, vol. 390, no. 1-2, pp. 344–349, 2005.

[7] G. A. Sweet, M. Brochu, R. L. Hexemer, I. W. Donaldson, and D. P. Bishop, "Consolidation of aluminum-based metal matrix composites via spark plasma sintering," *Materials Science and Engineering A*, vol. 648, pp. 123–133, 2015.

[8] V. Mohanavel, K. Ashraff Ali, S. Prasath, T. Sathish, and M. Ravichandran, "Microstructural and tribological characteristics of AA6351/Si3N4 composites manufactured by stir casting," *Journal of Materials Research and Technology*, vol. 9, no. 6, pp. 14662–14672, 2020.

[9] V. Mohanavel, S. Prasath, K. Yoganandam, B. Girma Tesemma, and S. Suresh Kumar, "Optimization of wear parameters of aluminium composites (AA7150/10 wt%WC) employing Taguchi approach," *Materials Today Proceedings*, vol. 33, no. 7, pp. 4742–4745, 2020.

[10] A. Kumar Sharma, R. Bhandari, A. Aherwar, R. Rimašauskienė, and C. Pinca-Bretotean, "A study of advancement in application opportunities of aluminum metal matrix composites," *Materials Today Proceedings*, vol. 26, no. 2, pp. 2419–2424, 2020.

[11] Y. Du, S. Li, K. Zhang, and K. Lu, "BN/Al composite formation by high-energy ball milling," *Scripta Materialia*, vol. 36, no. 1, pp. 7–14, 1997.

[12] M. Song, "Effects of volume fraction of SiC particles on mechanical properties of SiC/Al composites," *Transactions of Nonferrous Metals Society of China*, vol. 19, no. 6, pp. 1400–1404, 2009.

[13] M. Ebisawa, T. Hara, T. Hayashi, and H. Ushio, *Production Process of Metal Matrix Composite (MMC) Engine Block*, SAE Technical Paper 910835, Warrendyle, PA, USA, 1991.

[14] W. H. Hunt, "Aluminium metal matrix composites today," *Materials Science Forum*, vol. 331–337, pp. 71–84, 2000.

[15] B. Guo, M. Song, Y. Jianghong, N. Song, T. Shen, and Y. Du, "Improving the mechanical properties of carbon nanotubes reinforced pure aluminium matrix composites by achieving nonequilibrium interface," *J Mater Des*, vol. 120, pp. 56–65, 2017.

[16] B. Chen and K. Kondoh, "Sintering behaviours of carbon nanotubes-aluminium powder composites," *J Metall*, vol. 6, no. 9, p. 213, 2016.

[17] A. M. K. Esawi, K. Morsi, A. Sayed, M. Taher, and S. Lanka, "Effect of carbon nanotube (CNT) content on the mechanical properties of CNT-reinforced aluminium composites," *Composites Science and Technology*, vol. 70, no. 16, pp. 2237–2241, 2010.

[18] S. C. Tjong, "Recent progress in the development and properties of novel metal matrix nanocomposites reinforced with carbon nanotubes and graphene nanosheets," *Materials Science and Engineering: R: Reports*, vol. 74, no. 10, pp. 281–350, 2013.

[19] J. A. Jeffrey, S. S. Kumar, P. Hariharan, M. Kamesh, and A. M. Raj, "Production and assessment of AZ91 reinforced with nano SiC through stir casting process," *Inside MS*, vol. 1048, pp. 9–14, 2022.

[20] C. P. Reip and G. Sauthoff, "Deformation behaviour of the intermetallic phase Al3Nb with DO22 structure and of Al3Nb-base alloys: Part I. Physical properties and short-term behaviour," *Intermetallics*, vol. 1, no. 3, pp. 159–169, 1993.

[21] K. E. Thomson, D. Jiang, W. Yao, R. O. Ritchie, and A. K. Mukherjee, "Characterization and mechanical testing of alumina-based Nano composites reinforced with niobium and/or carbon nanotubes fabricated by spark plasma sintering," *Acta Materialia*, vol. 60, no. 2, pp. 622–632, 2012.

[22] K. Sairam, J. K. Sonber, T. S. R. C. H. Murthy et al., "Influence of spark plasma sintering parameters on densification and mechanical properties of boron carbide," *International Journal of Refractory Metals and Hard Materials*, vol. 42, pp. 185–192, 2014.

[23] R. Casati and M. Vedani, "Metal matrix composites reinforced by Nano particles- a review," *Metals*, vol. 4, no. 1, pp. 65–83, 2014.

[24] R. Reddy, "Processing of Nano scale materials," *Reviews on advanced Materials Science*, vol. 5, pp. 121–133, 2003.

[25] L. Wang, J. Zhang, and W. Jiang, "Recent development in reactive synthesis of nanostructured bulk materials by spark plasma sintering," *International Journal of Refractory Metals and Hard Materials*, vol. 39, pp. 103–112, 2013.

[26] I. u H. Toor, J. Ahmed, M. A. Hussein, and N. Al-Aqeeli, "Optimization of process parameters for spark plasma sintering of Nano-structured ferritic Fe-18Cr-2Si alloy," *Powder Technology*, vol. 299, pp. 62–70, 2016.

[27] I. Sulima, L. Jaworska, and P. Figiel, "Influence of processing parameters and different content of Tib2 ceramics on the properties of composites sintered by high pressure -high temperature (HP-ht) method," *Archives of Metallurgy and Materials*, vol. 59, no. 1, pp. 205–209, 2014.

[28] K. A. Ismaila, S. Nouari, F. H. Syed, and A. A. Nasser, "Microstructure and properties of spark plasma sintered Aluminium containing 1 wt. % SiC nanoparticles," *J Metals*, vol. 5, 2015.

[29] C. Kung, T. T. Liao, K. H. Tseng, K. Y. Chen, and M. S. Chuang, "The influences of powder mixing process on the quality of W-cu composites," *Transactions of the Canadian Society for Mechanical Engineering*, vol. 33, no. 3, pp. 361–375, 2009.

[30] K. R. Ranjit and N. D. Suren, "Design of experiments (DOE) using the taguchi approach," 2001, http://Nutek-us.com/wp-s4d.html.

[31] N. Raghunath and P. M. Pandey, "Improving accuracy through shrinkage modelling by using Taguchi method in selective laser sintering," *International Journal of Machine Tools and Manufacture*, vol. 47, no. 6, pp. 985–995, 2007.

[32] S. K. Das and P. Sahoo, "Tribological characteristics of electroless Ni–B coating and optimization of coating parameters using Taguchi based grey relational analysis," *Materials & Design*, vol. 32, no. 4, pp. 2228–2238, 2011.

[33] J. Rajaparthiban, M. Aswin, A. Abinaya et al., "Parametric analysis and simulation of surface roughness and tool flank wear in machining of low carbon alloy steel," *Materials Today Proceedings*, vol. 59, pp. 1457–1462, 2022.

[34] M. B. Shongwe, S. Diouf, M. O. Durowoju, and P. A. Olubambi, "Effect of sintering temperature on the microstructure and mechanical properties of Fe30%Ni alloys produced by spark plasma sintering," *Journal of Alloys and Compounds*, vol. 649, no. 9, pp. 824–832, 2015.

[35] Z. Zang, A. Nakamura, and J. Temmyo, "Single cuprous oxide films synthesized by radical oxidation at low temperature for PV applica- tion," *Optics Express*, vol. 21, no. 9, pp. 11448–11456, 2013.

[36] Z. Zang, A. Nakamura, and J. Temmyo, "Nitrogen doping in cuprous oxide films synthesized by radical oxidation at low temperature," *Materials Letters*, vol. 92, pp. 188–191, 2013.

[37] J. M. Ullbrand, J. M. Cordoba, J. M. Tamayo-Ariztondo et al., "Thermomechanical properties of copper-carbon nanofibre composites prepared by spark plasma sintering and hot pressing," *Composites Science and Technology*, vol. 70, no. 16, pp. 2263–2268, 2010.

[38] M. Muhammad and S. Muhammad, "Carbon nanotube-reinforced aluminium composite produced by induction melting," *Journal of Applied Research and Technology*, vol. 14, pp. 215–224, 2016.